Estimation of Frequency Response Functions by Random Decrement

Brincker, Rune; Asmussen, J. C.

Publication date:
1995

Document Version
Early version, also known as pre-print

INSTITUTTET FOR BYGNINGSTEKNIK
DEPT. OF BUILDING TECHNOLOGY AND STRUCTURAL ENGINEERING
AALBORG UNIVERSITET • AUC • AALBORG • DANMARK

FRACTURE & DYNAMICS
PAPER NO. 67

To be presented (partly) at the 14th International Modal Analysis Conference
Dearborn, Michigan, USA, February 12-15, 1996

J. C. ASMUSSEN, R. BRINCKER
ESTIMATION OF FREQUENCY RESPONSE FUNCTIONS BY RANDOM DECREMENT
DECEMBER 1995 ISSN 1395-7953 R9532

The FRACTURE AND DYNAMICS papers are issued for early dissemination of research results from the Structural Fracture and Dynamics Group at the Department of Building Technology and Structural Engineering, University of Aalborg. These papers are generally submitted to scientific meetings, conferences or journals and should therefore not be widely distributed. Whenever possible reference should be given to the final publications (proceedings, journals, etc.) and not to the Fracture and Dynamics papers.

Printed at Aalborg University

INSTITUTTET FOR BYGNINGSTEKNIK
DEPT. OF BUILDING TECHNOLOGY AND STRUCTURAL ENGINEERING
AALBORG UNIVERSITET • AUC • AALBORG • DANMARK

FRACTURE & DYNAMICS
PAPER NO. 67

To be presented (partly) at the 14th International Modal Analysis Conference
Dearborn, Michigan, USA, February 12-15, 1996

J. C. ASMUSSEN, R. BRINCKER
ESTIMATION OF FREQUENCY RESPONSE FUNCTIONS BY RANDOM DECREMENT
DECEMBER 1995 ISSN 1395-7953 R9532

ESTIMATION OF FREQUENCY RESPONSE FUNCTIONS BY RANDOM DECREMENT

J.C. Asmussen & R. Brincker

Department of Building Technology and Structural Engineering
Aalborg University, Sohngaardsholmsvej 57, 9000 Aalborg, Denmark.

Abstract A method for estimating frequency response functions by the Random Decrement technique is investigated in this paper. The method is based on the auto and cross Random Decrement functions of the input process and the output process of a linear system. The Fourier transformation of these functions is used to calculate the frequency response functions. The Random Decrement functions are obtained by averaging time segments of the processes under given initial conditions. The method will reduce the leakage problem, because of the natural decay of the Random Decrement functions. Also, the influence of noise will be reduced since the FFT is applied to the signatures, where the noise is reduced by averaging. Finally, the proposed technique will typically be faster than the traditional method, where the FFT is applied to every data segment instead of applying the FFT just once to the final Random Decrement function. The method is demonstrated by a simulation study.

Nomenclature

a	Value of time series.
C_Y	Trig condition on Y.
D_{YY}	Auto RDD function.
D_{XY}	Cross RDD function.
$h, \mathbf{h}$	Impulse response function/matrix.
$H, \mathbf{H}$	Frequency response function/matrix.
L	RDD function length and length of input time segments to FFT.
M	Number of points in FRF.
N	Number of trig points.
t_i	Discrete time point.
Y, X	Stochastic processes.
y, x	Realizations of Y, X
$\dot{Y}, \dot{X}$	Time derivative of Y,X
v	Value of time-derivative of time series.
Z	Fourier transformation of D.
σ_Y	Standard deviation of Y
τ	RDD function length

1 Introduction

This paper deals with the estimation of frequency response functions (FRF) of linear systems using the Random Decrement (RDD) technique. It is known, that the Fourier transformation of the auto- and cross-correlation function of the input and output processes of a linear system can be used to estimate the FRF of the system, see Bendat & Piersol [1]. Vandiver et al. [2] proved that the RDD technique applied with the level crossing trig condition estimates the auto-correlation function of a time series on the assumption of a zero mean Gaussian process. This result was generalized by Brincker et al. [3], [4], who proved on the same assumption, that the RDD technique applied with a generally formulated trig condition estimates a weighted sum of the auto- and cross-correlation functions of two time series and their time derivative. This could e.g. be the load process and the response process of a linear system.

In Brincker [3] the idea of using the Fourier transformation of the RDD functions as a basis for estimating FRFs is presented. This new method is the topic of this paper. The method is demonstrated by a simulation study of a linear 3 degree of freedom system loaded by pink noise at the first degree of freedom. The precision of the approach is compared with results obtained from traditional modal analysis based on FFT of the simulated time series. Even though the speed of this method is one of the advantages, compared to traditional modal analysis, this topic is not considered in this paper. Only accuracy is considered.

The influence of the number of points in the FRF estimate and the number of points in the time series is investigated. A quality measure is used to compare the results from RDD estimation combined with FFT (RDD-FFT) with a traditional FFT based technique (FFT). The simulation study show that RDD-FFT is more reliable than FFT. The accuracy of the FFT estimate of the FRF strongly depends on the number of points in each transformation. Furthermore, the RDD-FFT method is less sensitive to noise.

2 Random Decrement Technique

The RDD technique is a method for estimating auto- and cross-correlation functions of Gaussian processes, Vandiver et al. [2], Brincker et al. [3], [4]. The auto and cross RDD functions of the processes X and Y are defined as:

$$D_{YY}(\tau) = E[Y(t+\tau)|C_{Y(t)}] \quad (1)$$

$$D_{XY}(\tau) = E[X(t+\tau)|C_{Y(t)}] \quad (2)$$

i.e. RDD functions are defined as the mean value of a process Y given some trig conditions $C_{Y(t)}$ or $C_{X(t)}$. For a time series, the estimates of the auto and cross RDD functions are obtained as the empirical mean.

$$\hat{D}_{YY}(\tau) = \frac{1}{N}\sum_{i=1}^{N} y(\tau + t_i)|C_{Y(t_i)} \quad (3)$$

$$\hat{D}_{XY}(\tau) = \frac{1}{N}\sum_{i=1}^{N} x(\tau + t_i)|C_{Y(t_i)} \quad (4)$$

Where N is the number of points fulfilling the trig condition. Alternatively, the RDD functions, D_{XX} and D_{YX} could be estimated. Any trig condition can be constructed from the basic trig condition given by the complete initial conditions.

$$C_{Y(t_i)} = [Y(t_i) = a \ \vee \ \dot{Y}(t_i) = v] \quad (5)$$

Assuming that X and Y are stationary zero-mean Gaussian processes, the trig condition eq. (5) applied in eq. (1) and eq. (2) will yield, Brincker et al. [3], [4].

$$D_{YY}(\tau) = \frac{R_{YY}}{\sigma_Y^2}\cdot a + \frac{R'_{YY}}{\sigma_{\dot{Y}}^2}\cdot v \quad (6)$$

$$D_{XY}(\tau) = \frac{R_{XY}}{\sigma_Y^2}\cdot a + \frac{R'_{XY}}{\sigma_{\dot{Y}}^2}\cdot v \quad (7)$$

where σ_Y and $\sigma_{\dot{Y}}$ denote the standard deviation of Y and the time derivative $\dot{Y}$ of Y, R and R' denote the auto- and cross-covariance and their time derivatives.

From eq. (6) and eq. (7) several trig conditions can be formulated, which only picks out either the correlation functions or the derivative of the correlation functions, see Brincker et al. [4]. However, in this paper only two different trig conditions are considered: The local extremum trig condition eq. (8) and trigging at zero crossings with positive slope, eq. (9).

$$C_{Y(t)} = [Y(t) > 0 \vee \dot{Y}(t) = 0] \quad (8)$$

$$C_{Y(t)} = [Y(t) = 0 \vee \dot{Y}(t) > 0] \quad (9)$$

Given the previous by mentioned assumptions of Y and X, the local extremum trig condition reduces eq. (6) and eq. (7) to:

$$D_{YY}(\tau) = \frac{R_{YY}}{\sigma_Y^2}\cdot a \qquad D_{XY}(\tau) = \frac{R_{XY}}{\sigma_Y^2}\cdot a \quad (10)$$

Using zero crossing with positive slope reduces eq. (6) and eq. (7) to:

$$D_{YY}(\tau) = \frac{R'_{YY}}{\sigma_{\dot{Y}}^2}\cdot v \qquad D_{XY}(\tau) = \frac{R'_{XY}}{\sigma_{\dot{Y}}^2}\cdot v \quad (11)$$

These trig conditions have the advantage of picking out only the auto/cross-covariance or the derivative of the auto/cross-covariance.

RDD functions are "born" unbiased, sometimes however, implementation of the trig condition might change it slightly, and thus some changes of the functions might take place that in some cases might appear as bias. These problems are not present in this investigation, since the presented technique will work unbiased for any trig condition. The only bias introduced is the leakage bias introduced by the FFT. Because of the decay of the RDD function, the influence of this bias will be less than for the traditional FFT.

3 Estimation of FRF

Consider a linear system with n degrees of freedom. The response, $\mathbf{Y}$, of the system to some load $\mathbf{X}$ is given by the convolution integral, if the initial conditions are zero or negligible

$$\mathbf{Y}(t) = \int_{-\infty}^{t} \mathbf{h}(t-\eta)\mathbf{X}(\eta)d\eta \quad (12)$$

Where $\mathbf{h}$ is the impulse response matrix. Assuming that any random force has been applied to the ith degree of freedom only, the response at the jth degree of freedom is:

$$Y_j(t) = \int_{-\infty}^{t} h_{ij}(t-\eta)X_i(\eta)d\eta \quad (13)$$

To calculate the conditional mean value, see eq. (1), the time variables t and η are substituted. Eq. (13) can then be rewritten in the following form:

$$Y_j(t+\tau) = \int_{-\infty}^{\tau} h_{ij}(\tau-\xi)X_i(\xi+t)d\xi \quad (14)$$

Assuming that the impulse response matrix is time invariant, the conditional mean value, eq. (1), of eq. (14) can be calculated as:

$$E[Y_j(t+\tau)|C_{Y_i(t)}] = \int_{-\infty}^{\tau} h(\tau-\xi)E[X_i(t+\xi)|C_{Y_i(t)}]d\xi \quad (15)$$

or

$$D_{Y_jY_i}(t+\tau) = \int_{-\infty}^{\tau} h(\tau-\xi)D_{X_iY_i}(t+\tau)d\xi \quad (16)$$

The Fourier transformation, $Z(\omega)$, of the RDD function $D(\tau)$ is defined as:

$$Z(\omega) = \frac{1}{2\pi}\int_{-\infty}^{\infty} D(\tau)e^{-i\omega\tau}d\tau \quad (17)$$

Applying this definition to the time domain formulation eq. (16) together with the convolution theorem yields:

$$Z_{Y_jY_i}(\omega) = H_{ij}(\omega)Z_{X_iY_i}(\omega) \quad (18)$$

If the trig condition is applied to the load process of the system, an alternative formulation is obtained.

$$Z_{Y_jX_i}(\omega) = H_{ij}(\omega)Z_{X_iX_i}(\omega) \quad (19)$$

Eq. (18) and eq. (19) show that the Fourier transformation of the RDD functions can be used for estimation of the frequency response matrix of a linear system. The method is very similar to traditional modal analysis, were the frequency response matrix is estimated from the Fourier transformation of the measured load X and the measured response Y. The method has several advantages compared to traditional modal analysis. Since the RDD technique averages out the random errors before the Fourier transformation, the technique is expected to be less sensitive to noise. Furthermore, if the length of the RDD function is chosen long enough, the decay will reduce leakage. Dependent on the length of the RDD functions, the number of trig points and the length of the measured time series, this method might be somewhat faster than traditional modal analysis.

4 Simulation of 3DOF System

The purpose of this simulation study is to illustrate the application of the method for estimating FRF's of a multi-degree-of-freedom system. The system is linear with the following mass and stiffness matrices.

$$\mathbf{M} = \begin{bmatrix} 1 & 0 & 0 \\ 0 & 1 & 0 \\ 0 & 0 & 1 \end{bmatrix} \mathbf{K} = \begin{bmatrix} 400 & -300 & 0 \\ -300 & 600 & -300 \\ 0 & -300 & 350 \end{bmatrix} \quad (20)$$

The system is Raleigh damped with the damping matrix:

$$\mathbf{C} = 0.4 \cdot \mathbf{M} + 0.0004 \cdot \mathbf{K} \quad (21)$$

The modal parameters from this system are:

$$\begin{bmatrix} f_1 \\ f_2 \\ f_3 \end{bmatrix} = \begin{bmatrix} 1.095 \\ 3.085 \\ 4.845 \end{bmatrix} \quad \begin{bmatrix} \zeta_1 \\ \zeta_2 \\ \zeta_3 \end{bmatrix} = \begin{bmatrix} 0.030 \\ 0.014 \\ 0.013 \end{bmatrix} \quad (22)$$

$$\Phi = \begin{bmatrix} 1.000 & 1.000 & 1.000 \\ 1.175 & 0.081 & -1.756 \\ 1.165 & -0.940 & 0.913 \end{bmatrix} \quad (23)$$

The system was loaded by a pink noise process at the first mass. The pink noise process was simulated by an ARMA(2,1)-model, Pandit [6]. The response of the system to this load is simulated using standard routines from the MATLAB CONTROL TOOLBOX, [7]. The sampling frequency was chosen as 15 Hz and 30000 points were simulated. All investigations in this paper were performed using the same time series, although mostly only the first part of the time series was used. Figure 1 show the first part of the load process and the corresponding response at the first mass.

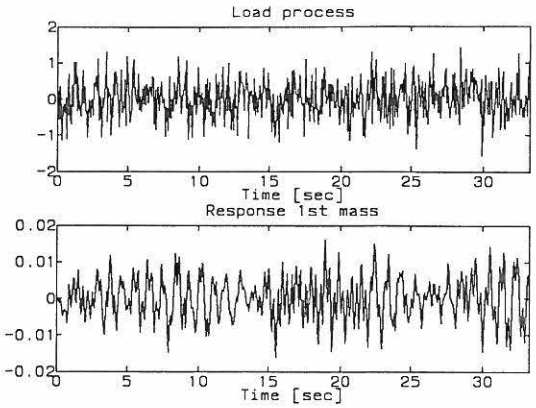

Figure 1: First part of simulated load process and the response at the first mass.

Figure 2 show the absolute value of the theoretical FRF (H_{11}) of the system and the load process.

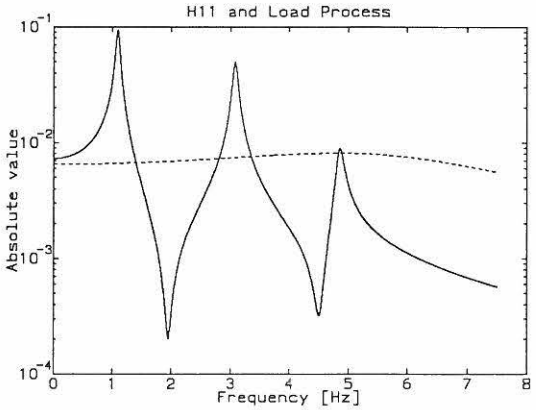

Figure 2: Theoretical absolute value of FRF, H_{11}, and theoretical absolute value of the load applied to mass 1.

The purpose of the investigations is to compare the accuracy of the RDD-FFT technique and the FFT. To have a measure for the accuracy of the different methods to the theoretical value of the FRF's, the following error function is defined:

$$error = \frac{1}{M} \sum_{i=1}^{M} |H_i - \hat{H}_i| \quad (24)$$

Where M is the number of points in the FRFs, H_i is the ith value of the theoretical FRF and $\hat{H}_i$ is the ith value of the estimated FRF. The error function is independent of the number of points in the FRFs. The influence of the length of the time series, the length of the RDD functions and the length of the time segments of the time series used by FFT in the estimation of the FRFs will be investigated. In the graphical presentation of the results L denotes the length of the RDD functions, which is always equal to the length of the time segments used as input for FFT. The following relation between L and the number of points in the FRFs exists: $L = 2 \cdot M + 1$. To illustrate the influence of L and the length of the time series the following quality measure is defined and used.

$$quality = \frac{1}{error} \quad (25)$$

Furthermore the influence of noise is investigated by adding a white noise sequence to the time series. The noise level is described by the signal-to-noise ratio defined as $\frac{\sigma_{noise}}{\sigma_{signal}}$. In order to use all information from the time series the RDD functions are estimated using a two step method. First the signatures are calculated as described in section 2, then the sign of the time series is changed. A new function is calculated, again according to section 2 and the average of these two functions is used as the resulting functions. Using this method all information from the time series is extracted.

5 Local Extremum Trigging

Figure 3 and figure 4 show the auto and 3 cross RDD functions estimated using the local extremum trig condition, eq. (5). The number of points used from the time series is 14000, and L has a size of 450 points. The trig condition is applied to the response of the first mass.

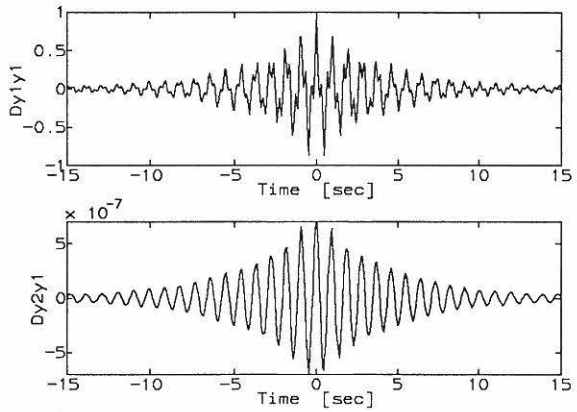

Figure 3: Auto, $D_{y_1y_1}$, and cross, $D_{y_2y_1}$ RDD signatures.

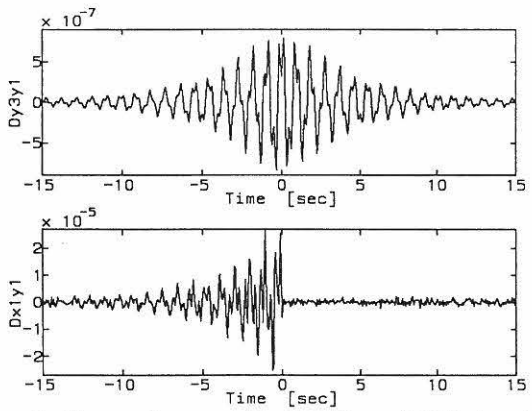

Figure 4: Cross, $D_{y_3y_1}$, and cross, $D_{x_1y_1}$ RDD signatures.

From these RDD functions it is expected to have a leakage-free estimate of the FRFs, because the functions are decaying to zero. Figure 5 - figure 10 show the absolute value and the phase of the theoretical FRF H_{11}, H_{21} and H_{31}, $\hat{H}_{11}$ $\hat{H}_{21}$ and $\hat{H}_{31}$ estimated using RDD-FFT and pure FFT.

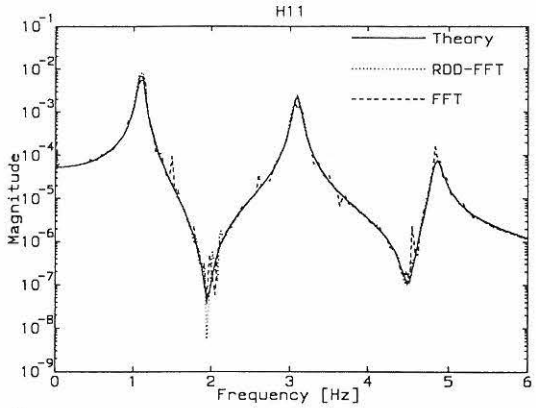

Figure 5: Magnitude of frequency response function, H_{11}.

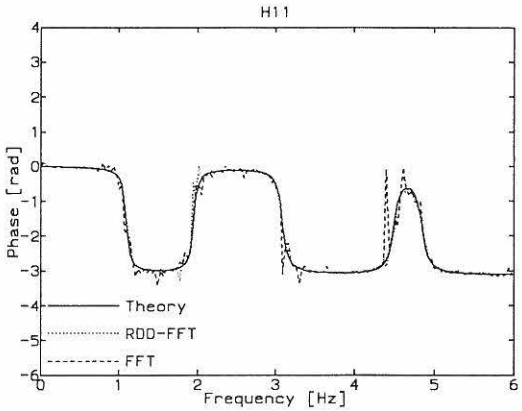

Figure 6: Phase of frequency response function, H_{11}.

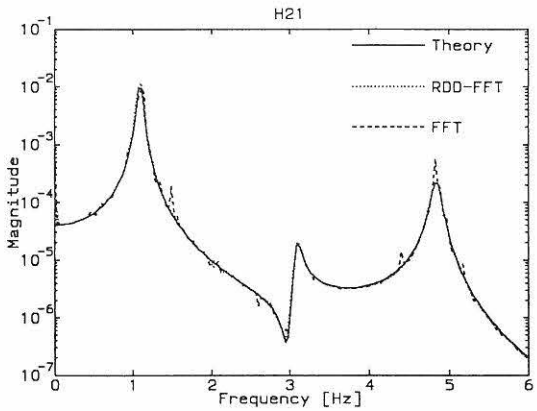

Figure 7: Magnitude of frequency response function, H_{21}.

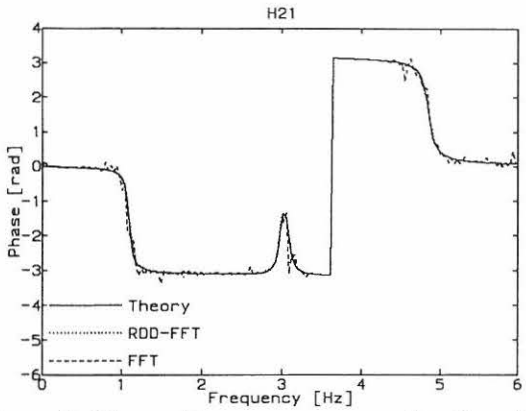

Figure 8: Phase of frequency response function, H_{21}.

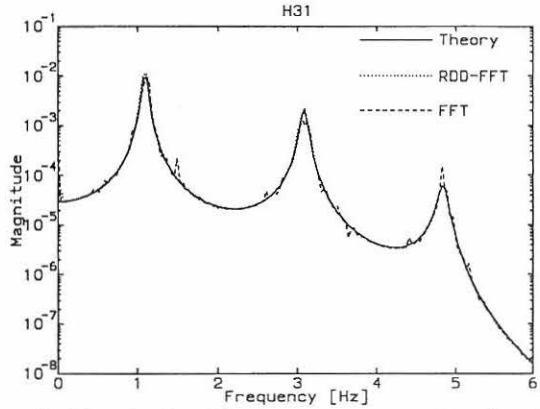

Figure 9: Magnitude of frequency response function, H_{31}.

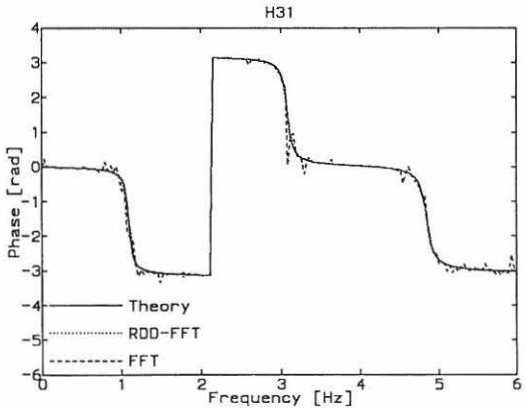

Figure 10: Phase of frequency response function, H_{31}.

Figure 11 - figure 34 show the quality calculuted as in eq. (25) of RDD-FFT and FFT with the size of the time series and L as variabels. The size of the time series is varied from 2000 points to 14000 points with steps of 1000 points. L is varied from 120 points to 512. Figure 11 - figure 16 show the quality estimated where no noise is added, figure 17 - figure 22 show the results with 1% noise added, figure 23 - figure 28 show the results with 3% noise added and finally figure 29 - figure 30 show the results with 10% noise added.

Figure 11 - figure 16 show results obtained from a noise-free time series.

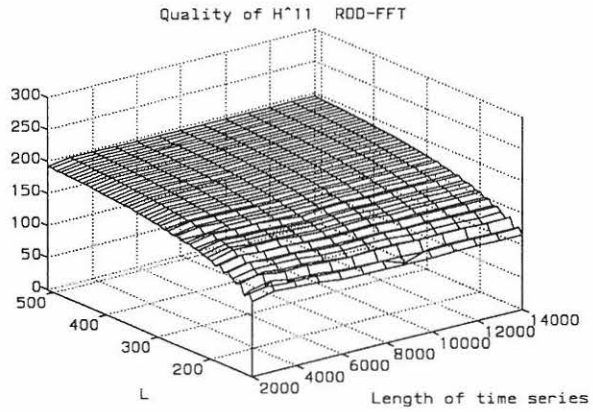

Figure 11: Quality of FRF H_{11} estimated by RDD-FFT.

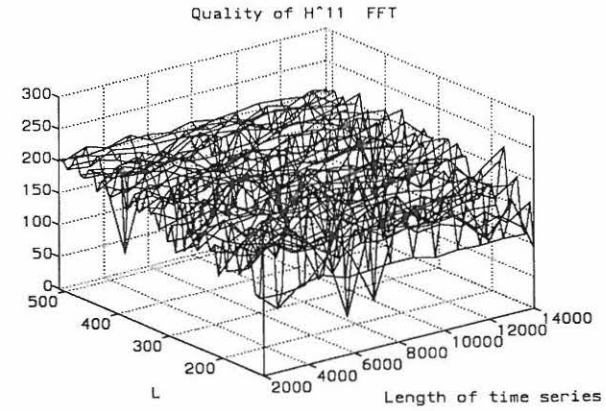

Figure 12: Quality of FRF H_{11} estimated by FFT.

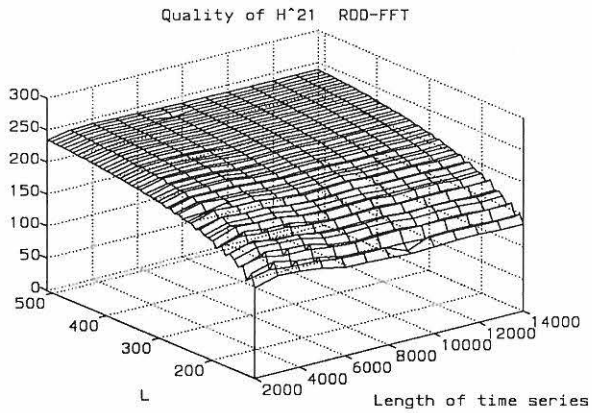

Figure 13: Quality of FRF H_{21} estimated by RDD-FFT.

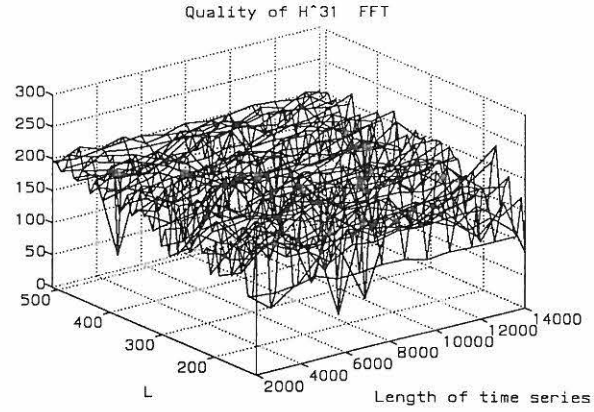

Figure 16: Quality of FRF H_{31} estimated by FFT.

Figure 17 - figure 22 show results obtained from a time series with 1% noise added.

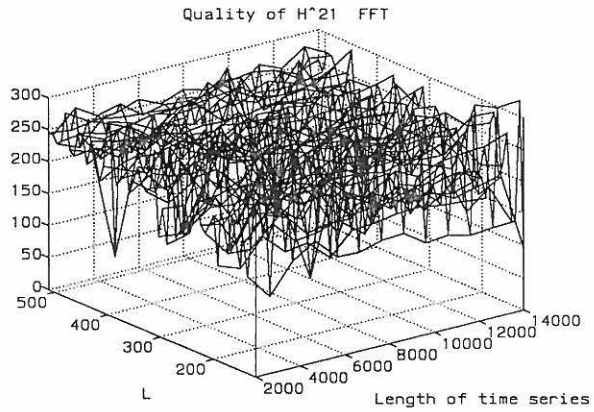

Figure 14: Quality of FRF H_{21} estimated by FFT.

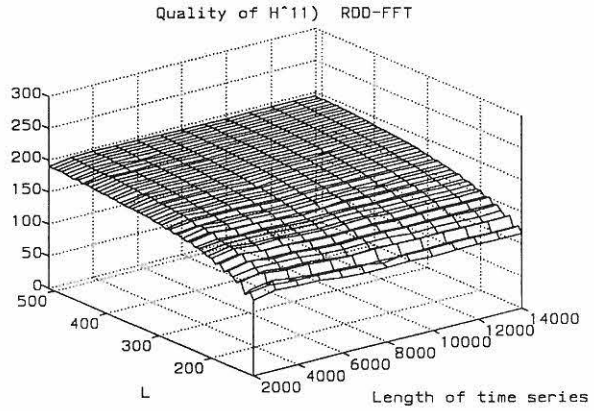

Figure 17: Quality of FRF H_{11} estimated by RDD-FFT.

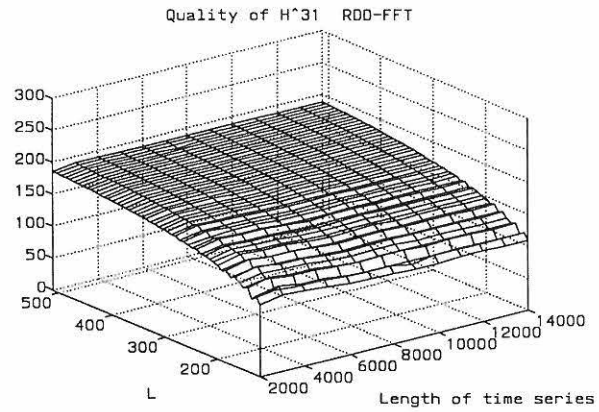

Figure 15: Quality of FRF H_{31} estimated by RDD-FFT.

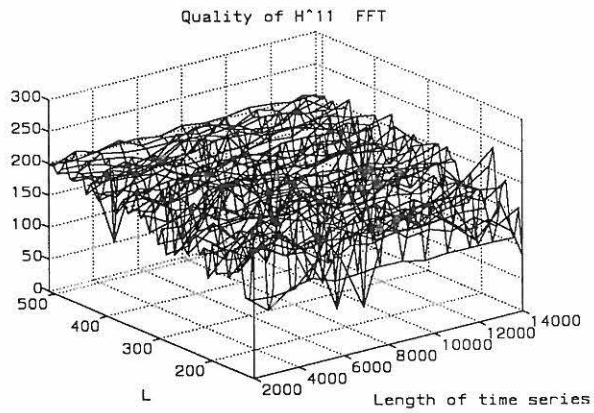

Figure 18: Quality of FRF H_{11} estimated by FFT.

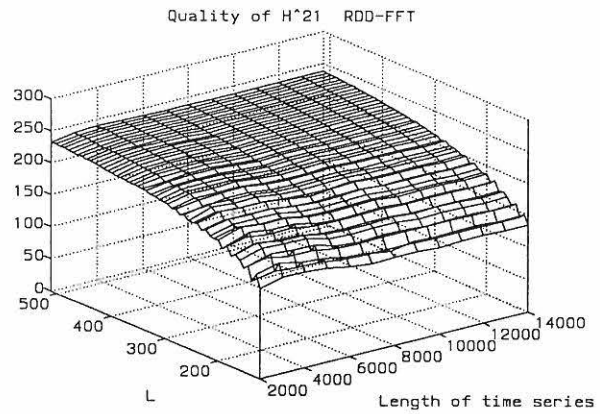

Figure 19: Quality of FRF H_{21} estimated by RDD-FFT.

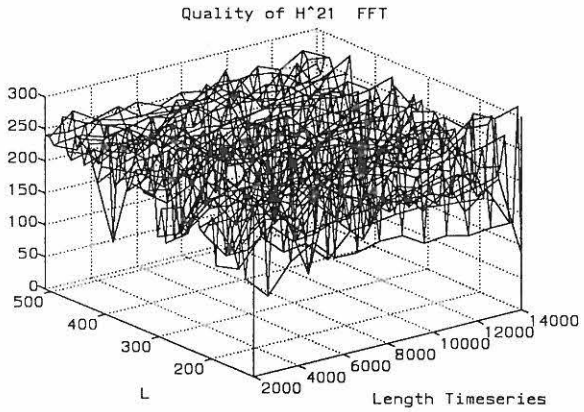

Figure 20: Quality of FRF H_{21} estimated by FFT.

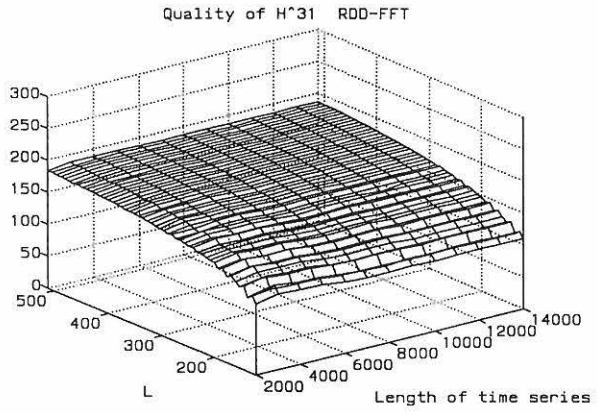

Figure 21: Quality of FRF H_{31} estimated by RDD-FFT.

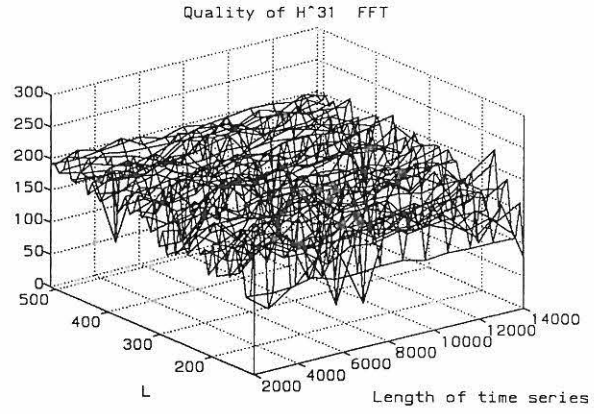

Figure 22: Quality of FRF H_{31} estimated by FFT.

Figure 23 - figure 34 show results obtained from a time series with 3% noise added.

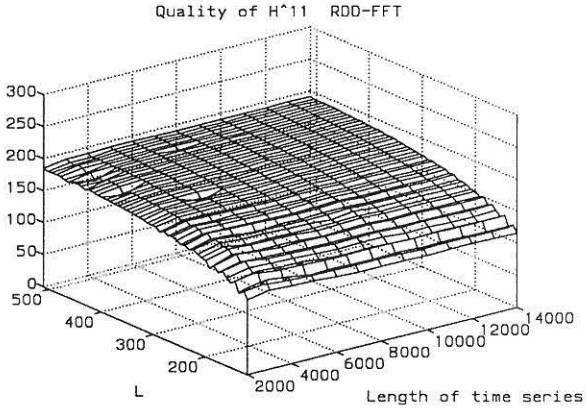

Figure 23: Quality of FRF H_{11} estimated by RDD-FFT.

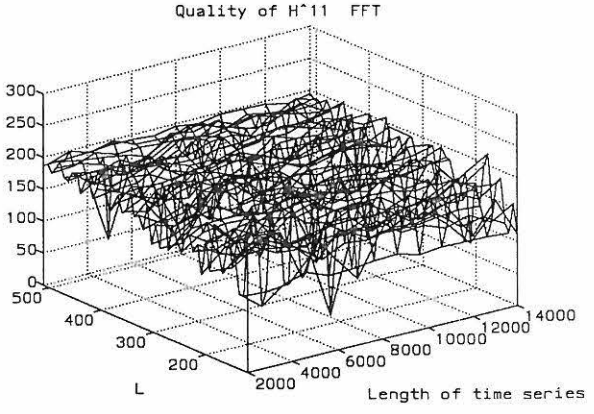

Figure 24: Quality of FRF H_{11} estimated by FFT.

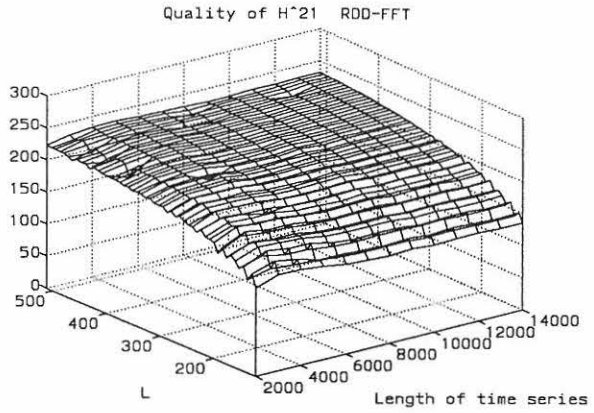

Figure 25: Quality of FRF H_{21} estimated by RDD-FFT.

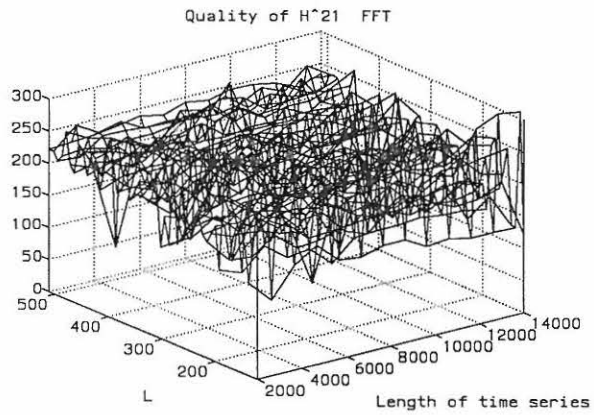

Figure 26: Quality of FRF H_{21} estimated by FFT.

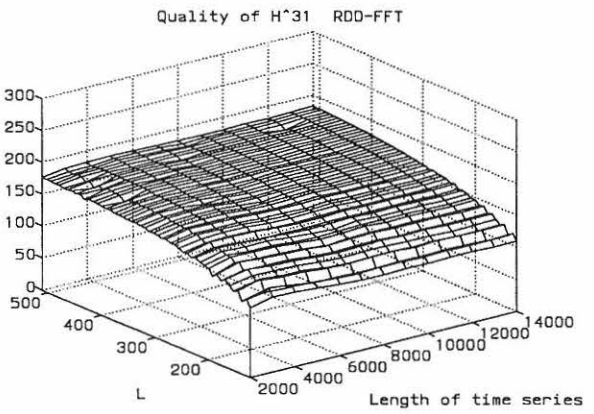

Figure 27: Quality of FRF H_{31} estimated by RDD-FFT.

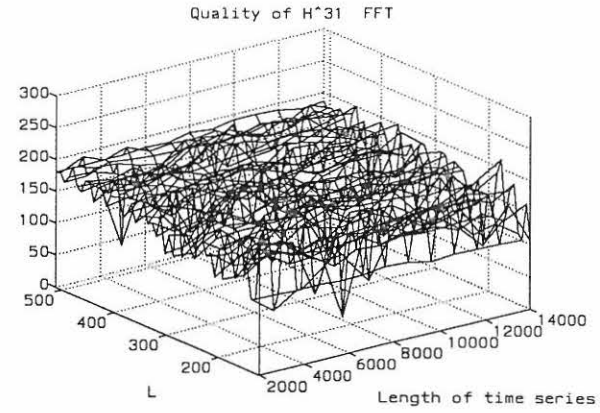

Figure 28: Quality of FRF H_{31} estimated by FFT.

Figure 23 - figure 34 show results obtained from a time series with 10% noise added.

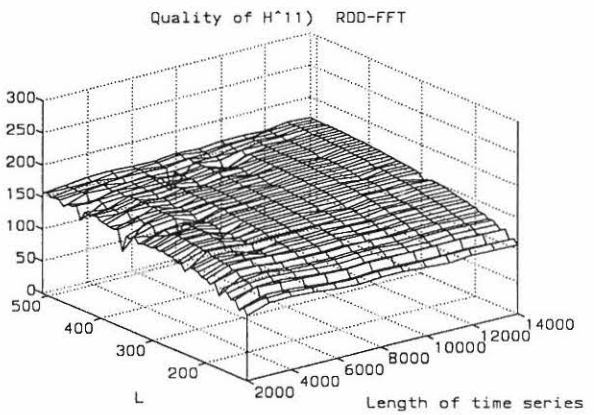

Figure 29: Quality of FRF H_{11} estimated by RDD-FFT.

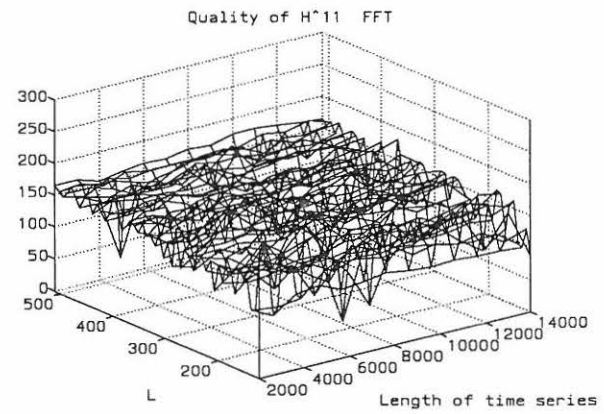

Figure 30: Quality of FRF H_{11} estimated by FFT.

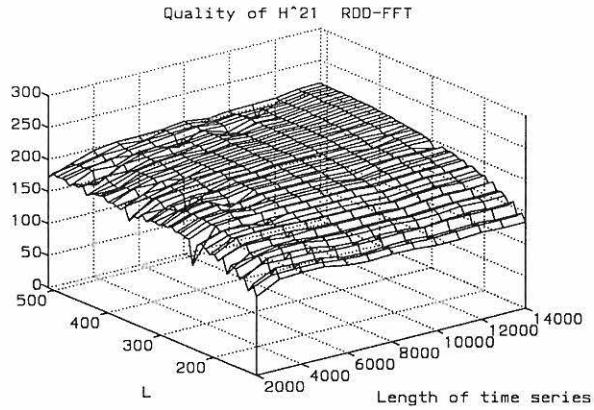

Figure 31: Quality of FRF H_{21} estimated by RDD-FFT.

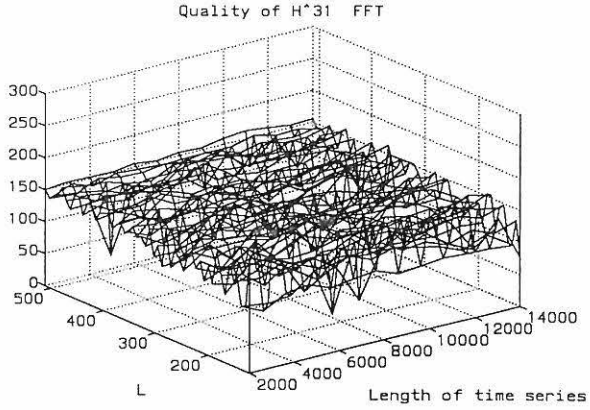

Figure 34: Quality of FRF H_{31} estimated by FFT.

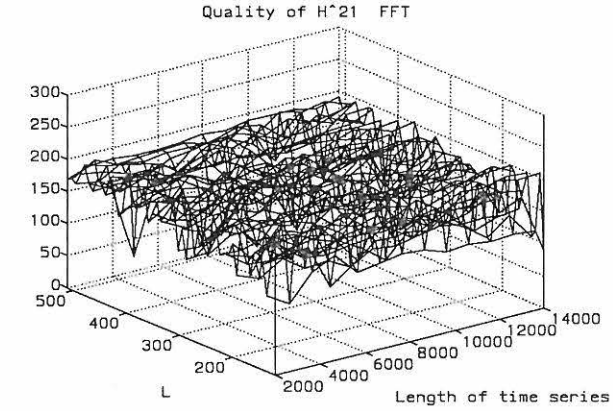

Figure 32: Quality of FRF H_{21} estimated by FFT.

The above figures show that the estimations using RDD-FFT and FFT are different. The RDD-FFT gives a smooth curve, while the FFT results in curves with a lot of pitfalls. Even with 10% noise in the time-series the RDD-FFT curves are smooth. This show that the RDD-FFT is more reliable. On average, the quality of the two methods is very alike.

Figure 35 - figure 37 show a comparison of RDD-FFT and FFT using 5000 points from the time series. The figures show the quality with 0%, 1%, 3% 10% noise added. The top lines correspond to analysis from a noise free time series while the bottom lines corresponds to a time series with 10 % noise added.

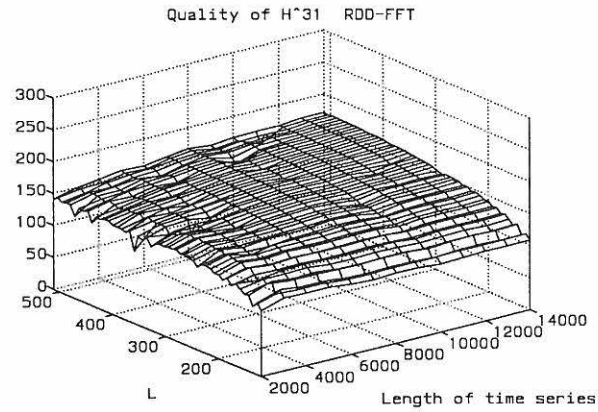

Figure 33: Quality of FRF H_{31} estimated by RDD-FFT.

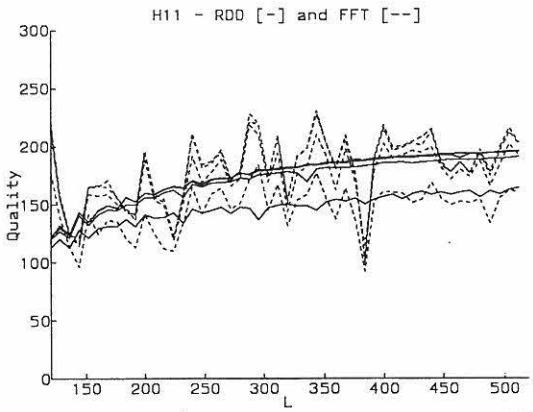

Figure 35: Quality of $\hat{H_{11}}$ estimated by RDD-FFT and FFT. 5000 points used.

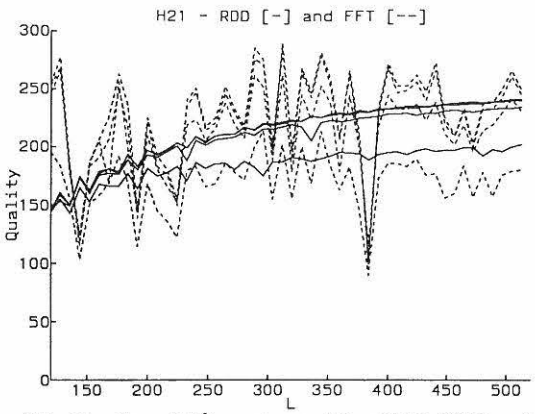

Figure 36: Quality of $\hat{H_{21}}$ estimated by RDD-FFT and FFT. 5000 points used.

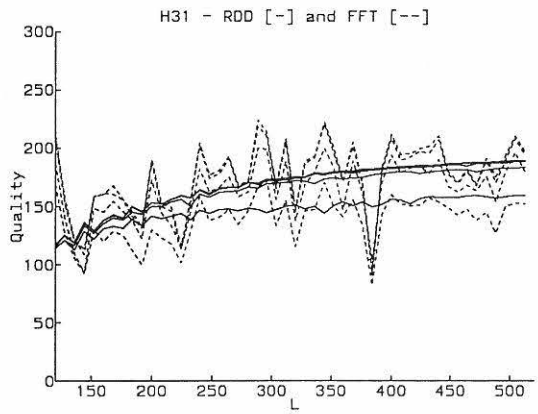

Figure 37: Quality of $\hat{H_{31}}$ estimated by RDD-FFT and FFT. 5000 points used.

Figure 38 - figure 40 show a comparison of RDD-FFT and FFT with 30000 points used from the time series. The figures show the quality with 0%, 1% and 3% noise added.

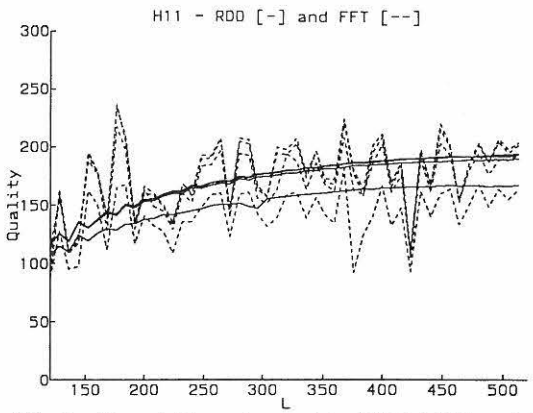

Figure 38: Quality of $\hat{H_{11}}$ estimated by RDD-FFT and FFT. 14000 points used.

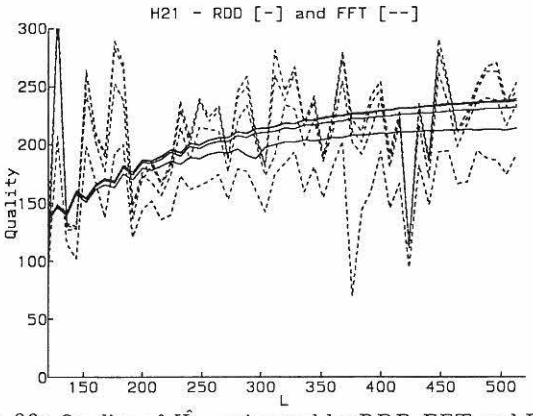

Figure 39: Quality of $\hat{H_{21}}$ estimated by RDD-FFT and FFT. 14000 points used.

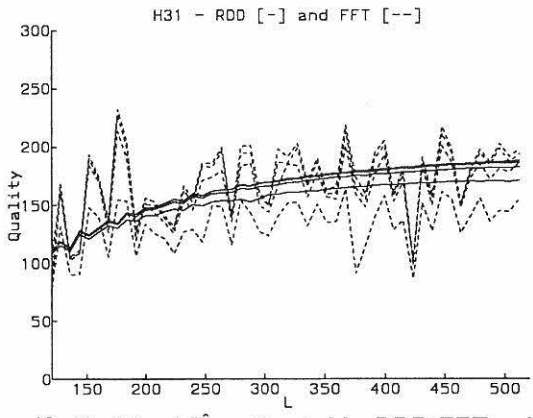

Figure 40: Quality of $\hat{H_{31}}$ estimated by RDD-FFT and FFT. 14000 points used.

Figure 41 - figure 43 show a comparison of RDD-FFT and FFT with 30000 points used from the time series. The figures show the quality with 0%, 1% and 3% noise added.

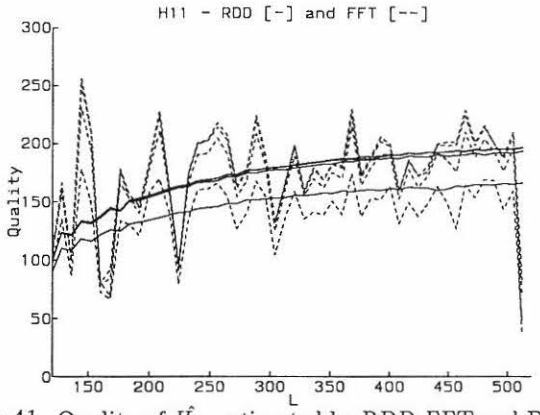

Figure 41: Quality of $\hat{H_{11}}$ estimated by RDD-FFT and FFT. 30000 points used.

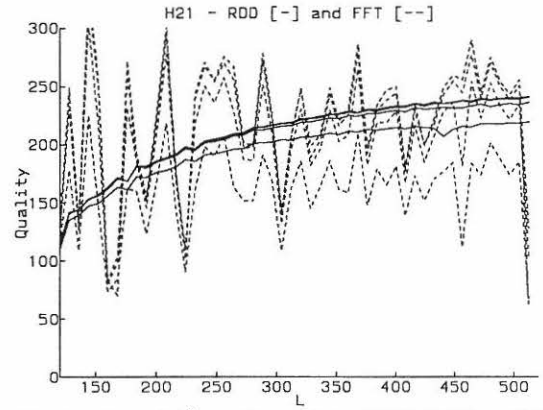

Figure 42: Quality of $\hat{H_{21}}$ estimated by RDD-FFT and FFT. 30000 points used.

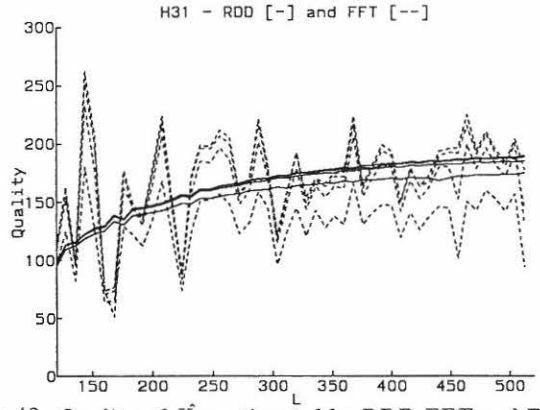

Figure 43: Quality of $\hat{H_{31}}$ estimated by RDD-FFT and FFT. 30000 points used.

Also for larger time series, it is seen that FFT fluctuates unpredictably. The influence of noise by the RDD-FFT method has decreased by using 30000 points compared to the results obtained using 5000 points. As expected, this indicates that more trig points average out noise. If the time series has a sufficient length, RDD-FFT is clearly less sensitive to noise compared to pure FFT.

6 Zero Crossing Trig Condition

Figure 44 and figure 45 show the auto and 3 cross RDD functions estimated using the zero crossing trig condition, eq. (5). The number of points in the time series 14000 points, and L has a size of 450 points. The trig condition is applied to the response of the first mass.

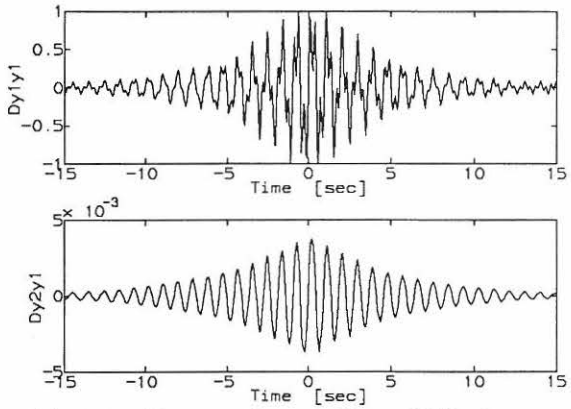

Figure 44: Auto, $D_{y_1y_1}$, and cross, $D_{y_2y_1}$ RDD signatures.

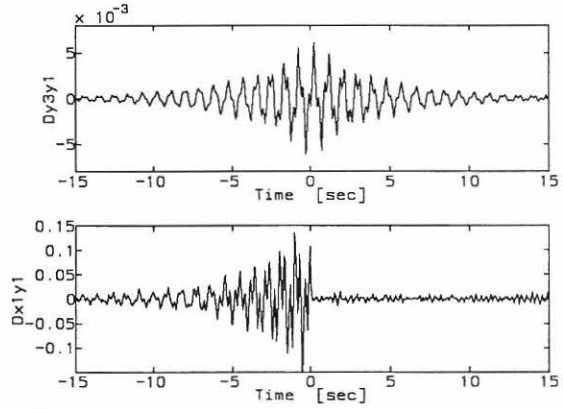

Figure 45: Cross, $D_{y_3y_1}$, and cross, $D_{x_1y_1}$ RDD signatures.

From these RDD functions it is expected to have a leakage-free estimate of the FRFs, because the functions are decaying to zero. Figure 46 - figure 51 show the absolute value and the phase of the theoretical FRF H_{11}, H_{21} and H_{31}, $\hat{H}_{11}$ $\hat{H}_{21}$ and $\hat{H}_{31}$ estimated using RDD-FFT and pure FFT.

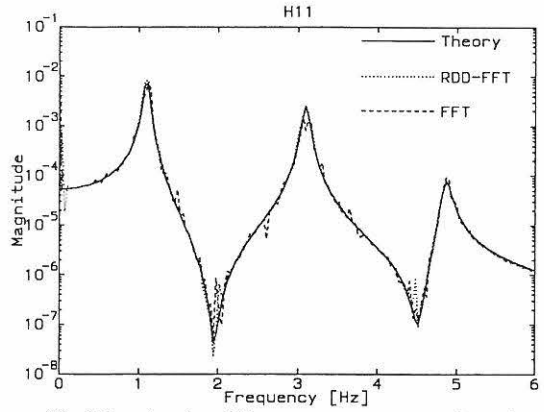

Figure 46: Magnitude of frequency response function, H_{11}.

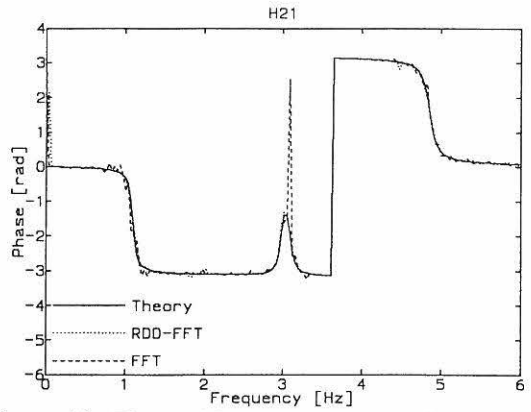

Figure 49: Phase of frequency response function, H_{21}.

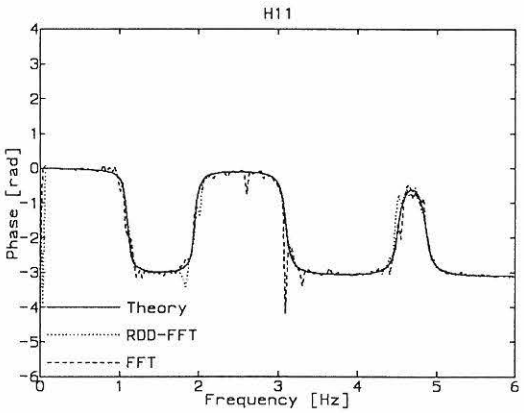

Figure 47: Phase of frequency response function, H_{11}.

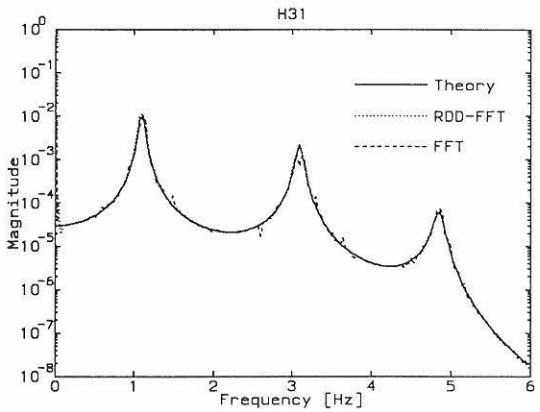

Figure 50: Magnitude of frequency response function, H_{31}.

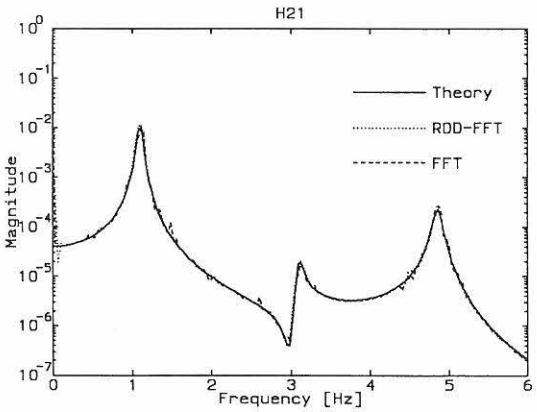

Figure 48: Magnitude of frequency response function, H_{21}.

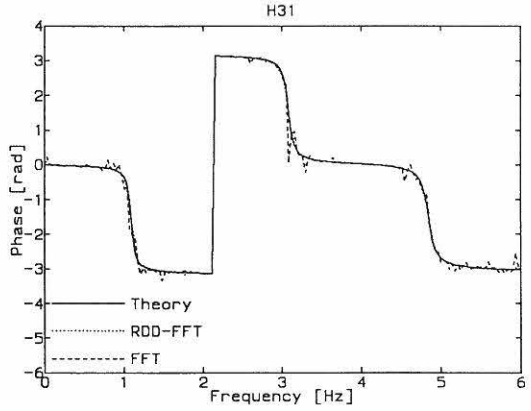

Figure 51: Phase of frequency response function, H_{31}.

Figure 52 - figure 75 show the quality calculated as in eq. (25) of RDD-FFT and FFT with the size of the time series and L as variabels. The size of the time series is varied from 2000 points to 14000 points with steps of 1000 points. L is varied from 120 to 512 points. Figure 52 - figure 57 show the quality estimated where no noise is added, figure 58 - figure

63 show the results with 1% noise added, figure 64 - figure 69 show the results with 3% noise added and finally figur 70 - figure 75 show the results with 10% noise added.

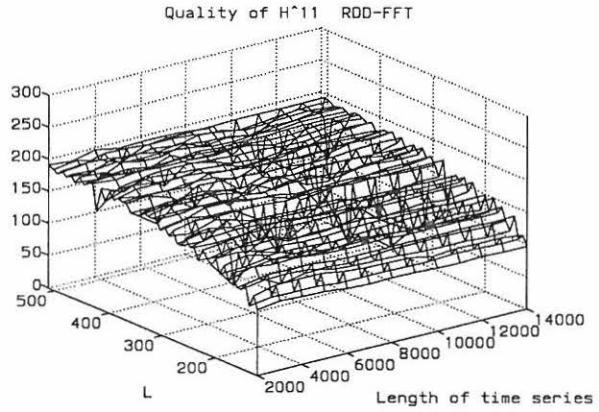

Figure 52: Quality of FRF H_{11} estimated by RDD-FFT.

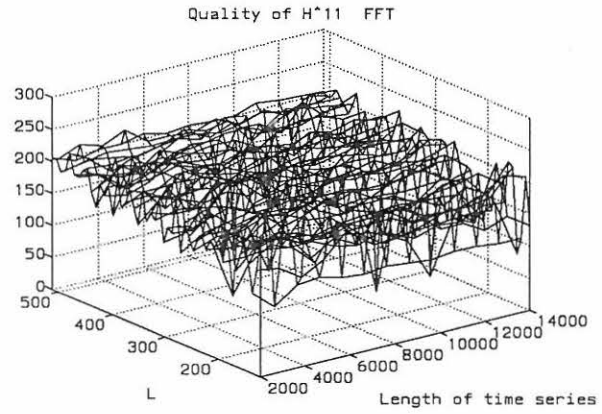

Figure 53: Quality of FRF H_{11} estimated by FFT.

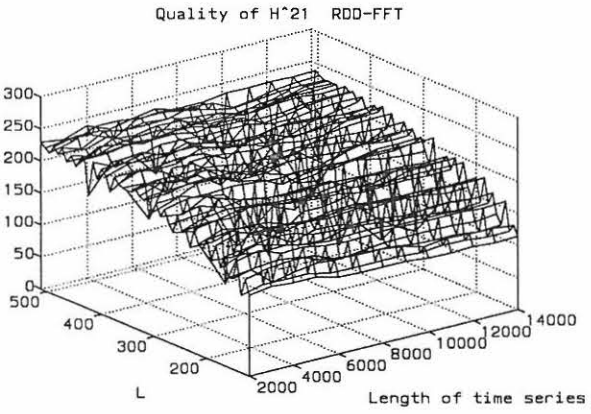

Figure 54: Quality of FRF H_{21} estimated by RDD-FFT.

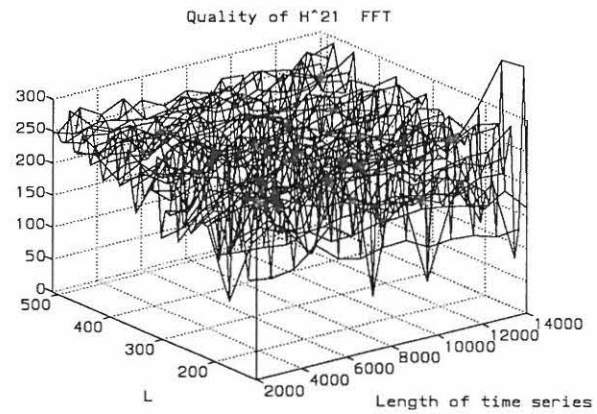

Figure 55: Quality of FRF H_{21} estimated by FFT.

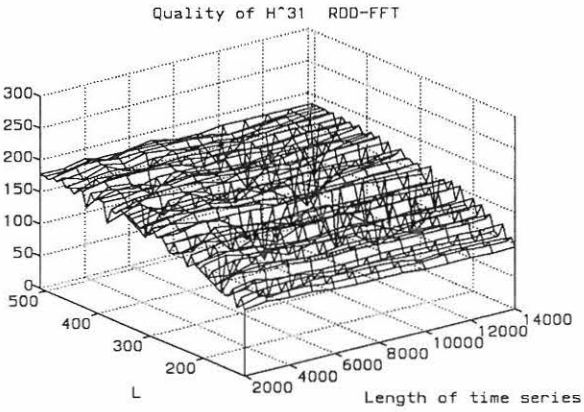

Figure 56: Quality of FRF H_{31} estimated by RDD-FFT.

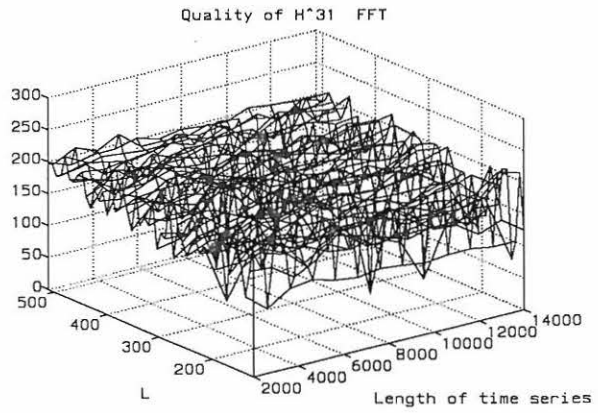

Figure 57: Quality of FRF H_{31} estimated by FFT.

Figure 58 - figure 63 show results obtained from a time series with 1% noise added.

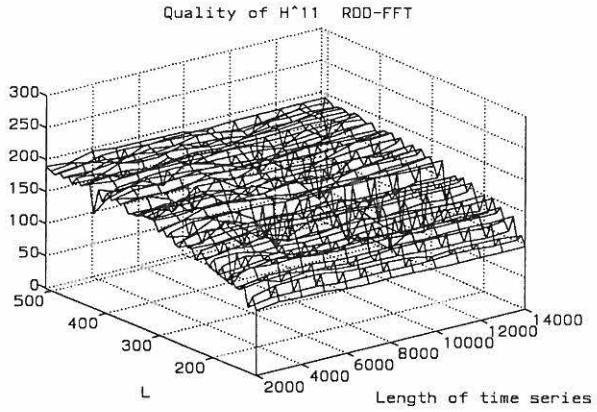

Figure 58: Quality of FRF H_{11} estimated by RDD-FFT.

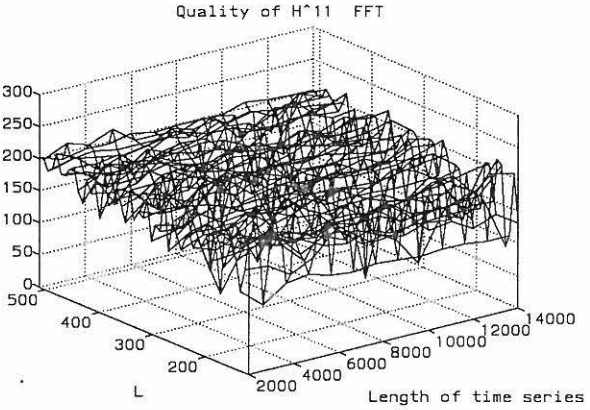

Figure 59: Quality of FRF H_{11} estimated by FFT.

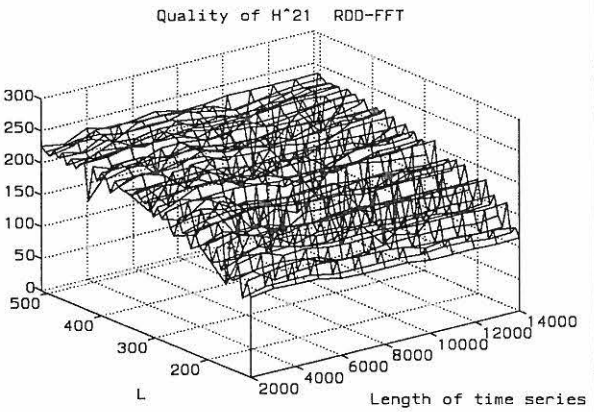

Figure 60: Quality of FRF H_{21} estimated by RDD-FFT.

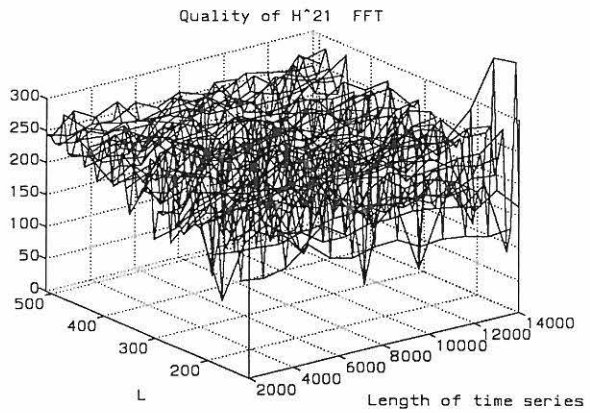

Figure 61: Quality of FRF H_{21} estimated by FFT.

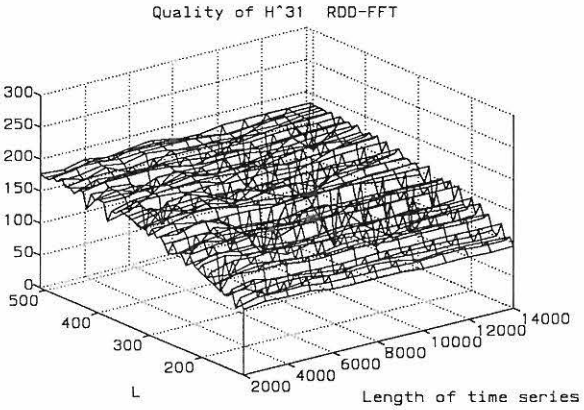

Figure 62: Quality of FRF H_{31} estimated by RDD-FFT.

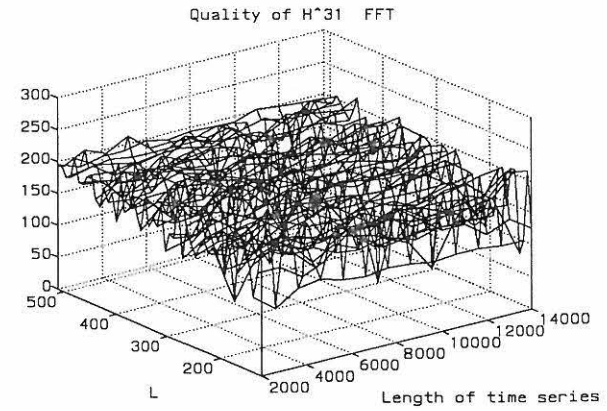

Figure 63: Quality of FRF H_{31} estimated by FFT.

Figure 58 - figure 63 show results obtained from a time series with 3% noise added.

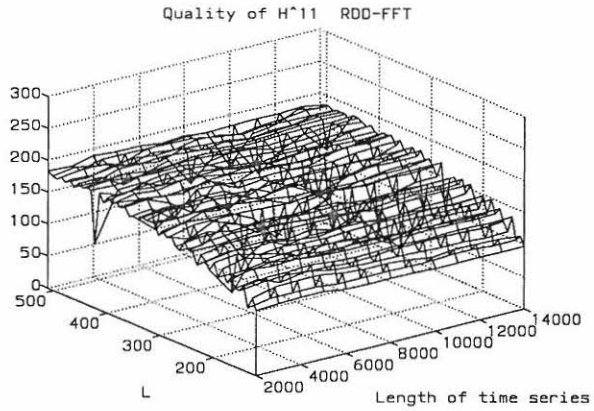

Figure 64: Quality of FRF H_{11} estimated by RDD-FFT.

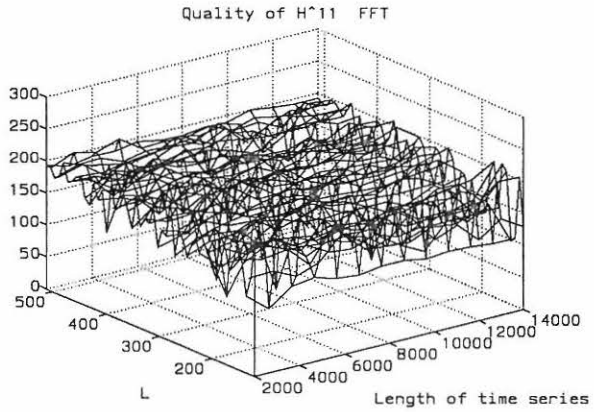

Figure 65: Quality of FRF H_{11} estimated by FFT.

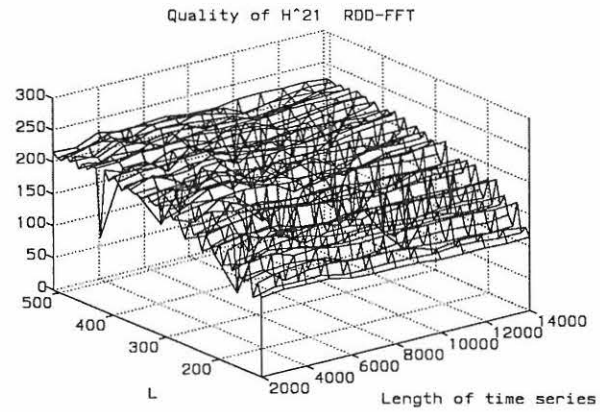

Figure 66: Quality of FRF H_{21} estimated by RDD-FFT.

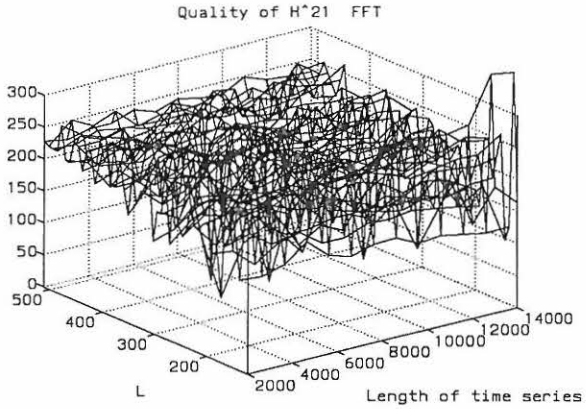

Figure 67: Quality of FRF H_{21} estimated by FFT.

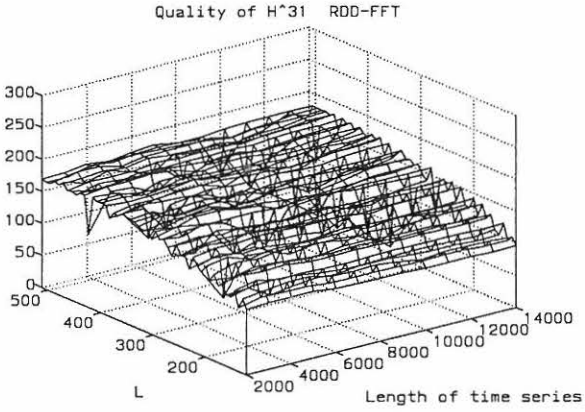

Figure 68: Quality of FRF H_{31} estimated by RDD-FFT.

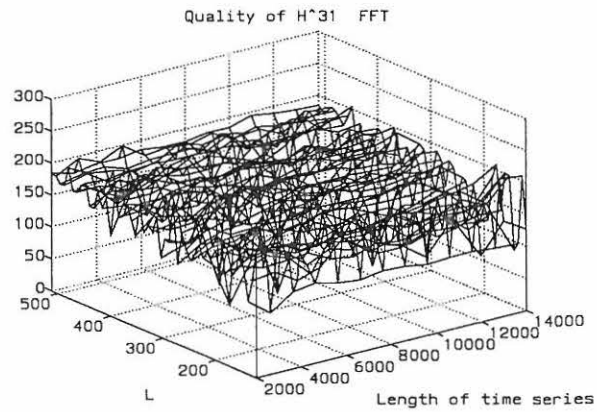

Figure 69: Quality of FRF H_{31} estimated by FFT.

Figure 58 - figure 63 show results obtained from a time series with 10% noise added.

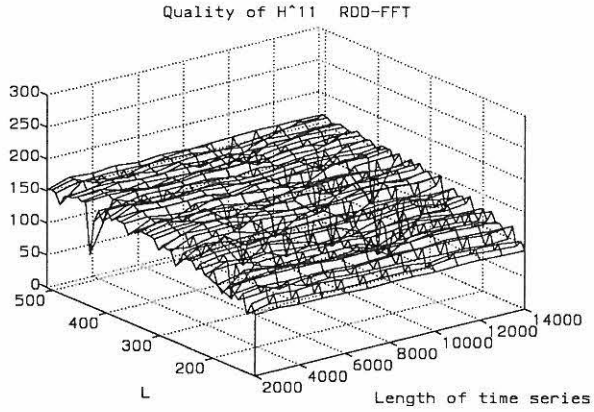

Figure 70: Quality of FRF H_{11} estimated by RDD-FFT.

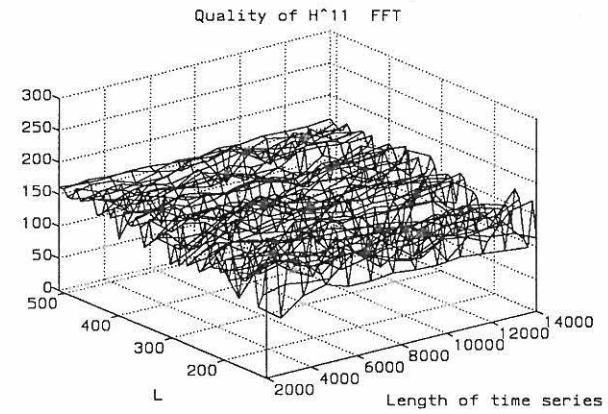

Figure 71: Quality of FRF H_{11} estimated by FFT.

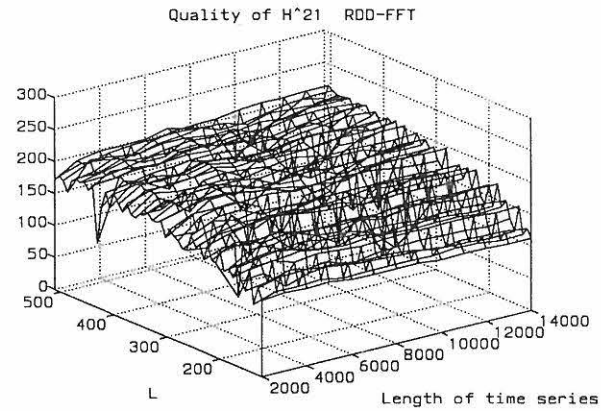

Figure 72: Quality of FRF H_{21} estimated by RDD-FFT.

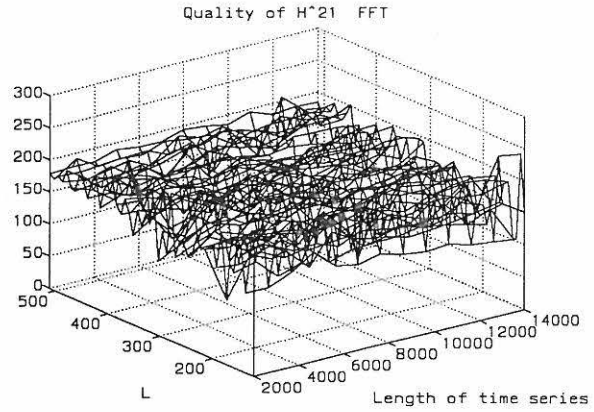

Figure 73: Quality of FRF H_{21} estimated by FFT.

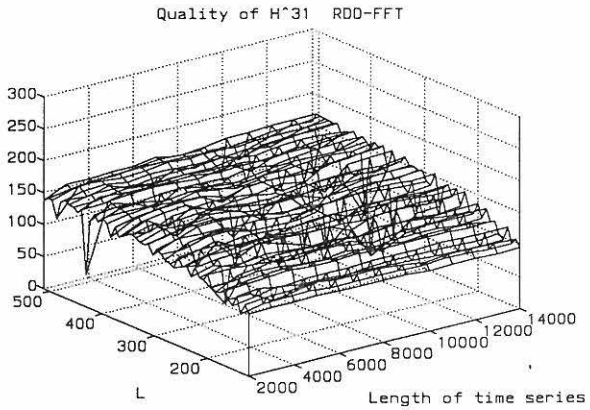

Figure 74: Quality of FRF H_{31} estimated by RDD-FFT.

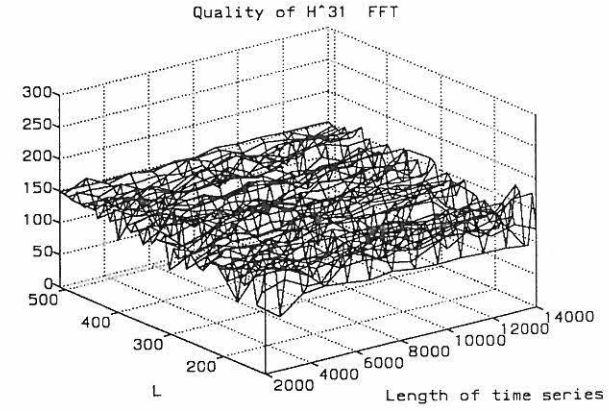

Figure 75: Quality of FRF H_{31} estimated by FFT.

Using the zero crossing trig condition the RDD-FFT estimation also includes a lot of pitfalls or variations with especially the function length. Although the variations from RDD-FFT

estimates are smother than the variations from pure FFT estimates, this trig condition cannot compete with the local extremum trig condition.

Figure 76 - figure 78 show a comparison of RDD-FFT and FFT using 5000 points from the time series. The figures show the quality with 0%, 1%, 3% and 10% noise added.

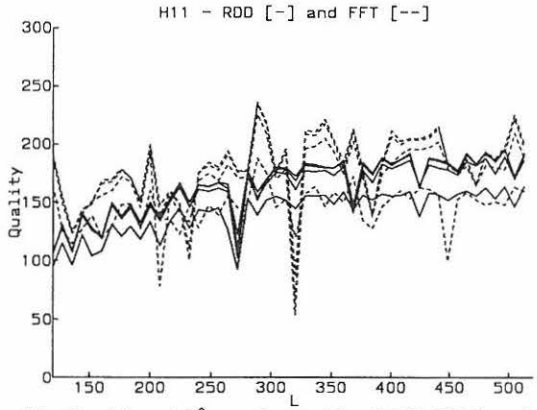

Figure 76: Quality of $\hat{H_{11}}$ estimated by RDD-FFT and FFT. 5000 points used.

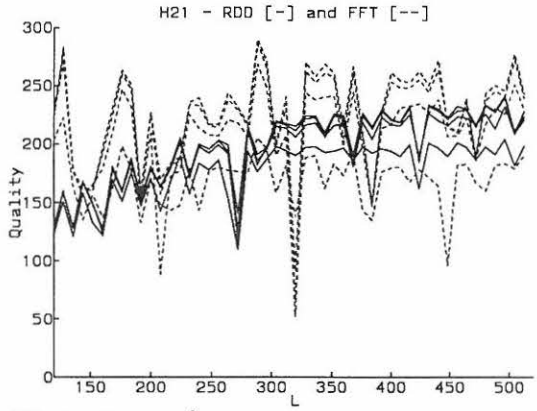

Figure 77: Quality of $\hat{H_{21}}$ estimated by RDD-FFT and FFT. 5000 points used.

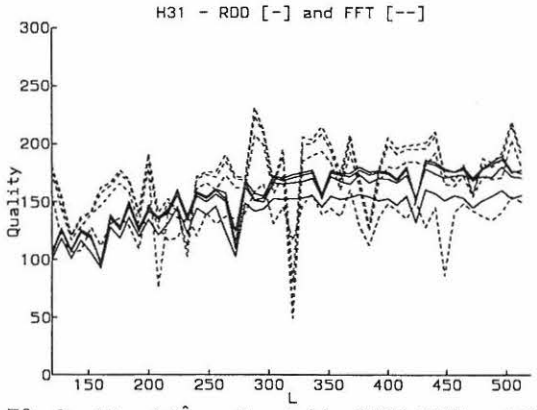

Figure 78: Quality of $\hat{H_{31}}$ estimated by RDD-FFT and FFT. 5000 points used.

Figure 79 - figure 81 show a comparison of RDD-FFT and FFT using 14000 points from the time series. The figures show the quality with 0%, 1%, 3% 10% noise added.

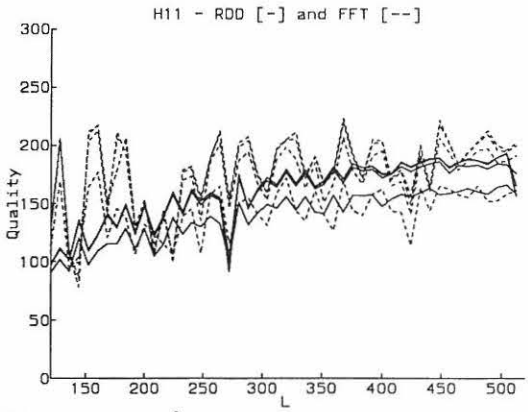

Figure 79: Quality of $\hat{H_{11}}$ estimated by RDD-FFT and FFT. 14000 points used.

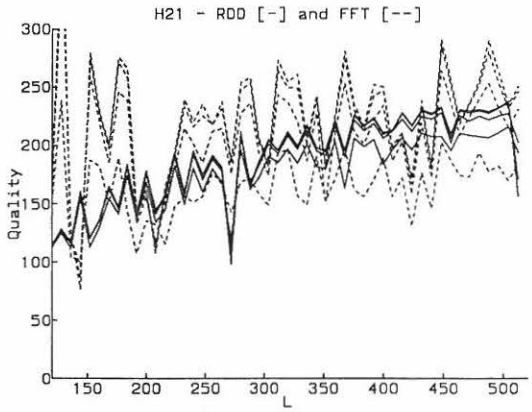

Figure 80: Quality of $\hat{H_{21}}$ estimated by RDD-FFT and FFT. 14000 points used.

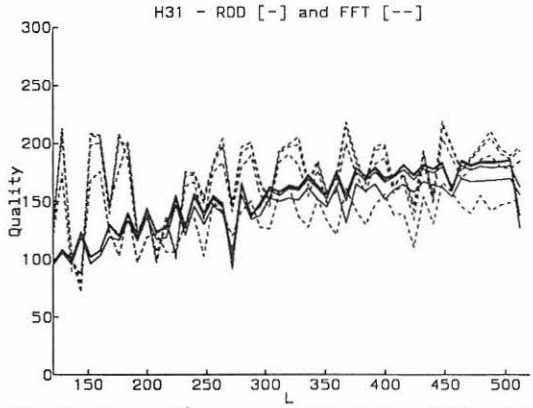

Figure 81: Quality of $\hat{H_{31}}$ estimated by RDD-FFT and FFT. 14000 points used.

Figure 82 - figure 84 show a comparison of RDD-FFT and FFT with 30000 points used from the time series. The figures show the quality with 0%, 1%, 3% 10% noise added.

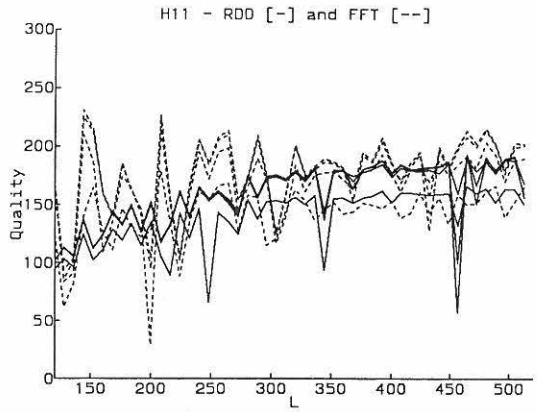

Figure 82: Quality of $\hat{H_{11}}$ estimated by RDD-FFT and FFT. 30000 points used.

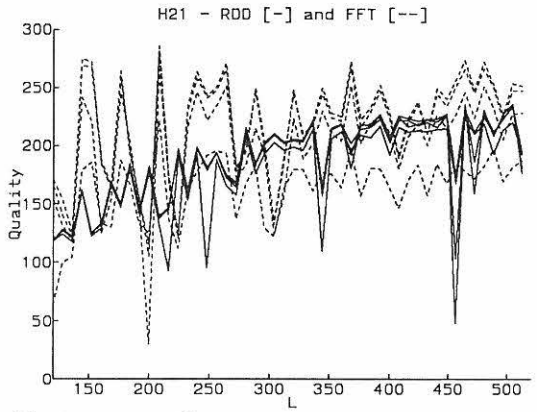

Figure 83: Quality of $\hat{H_{21}}$ estimated by RDD-FFT and FFT. 30000 points used.

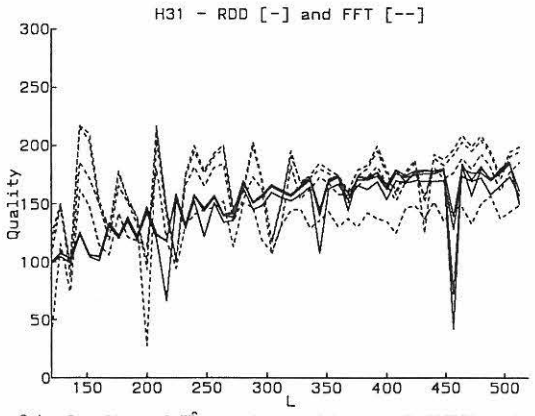

Figure 84: Quality of $\hat{H_{31}}$ estimated by RDD-FFT and FFT. 30000 points used.

From figure 76 - figure 84 it is concluded that RDD-FFT is less sensitive to noise compared with pure FFT. The disadvantage of the zero crossing trig condition is that the quality is far more dependent on the function length than the local extremum trig condition.

7 Conclusion

A new method for performing modal analysis has been investigated. The method is based on FFT of RDD functions. Two different trig conditions: Local extremum and zero crossing have been compared. The results shows that the local extremum trig condition is the most reliable trig condition. The comparison is based on variations of the length of the analysed time series and the length of the RDD functions equal to the length of the time segments used by FFT. The precision of the trig conditions is investigated by defining a quality measure. No attention is given to the estimation time, but the RDD-FFT technique will be faster than pure FFT in most applications.

The RDD-FFT method is also compared with traditional modal analysis based on FFT. From the quality of the estimations, it is concluded that RDD-FFT is more reliable than FFT. Even though the average quality of the two methods is very alike. Furthermore, it seems that RDD-FFT is less sensitive to noise. Especially if a long time series is used, RDD-FFT averages out noise. To have more information about RDD-FFT, several other trig conditions should be investigated. The estimation time of both methods should also be investigated as a function of the quality.

8 Acknowledgement

The Danish Technical Research Council is gratefully acknowledged.

References

[1] Bendat, J.S. & Piersol, A.G. *Random Data - Analysis and Measurement Procedures.* John Wiley & Sons, New York 1986, second edition

[2] Vandiver, J.K., Dunwoody, A.B., Campbell, R.B. & Cook, M.F. *A Mathematical Basis for the Random Decrement Signature Analysis Technique.* Journal of Mechanical Design, Vol. 104, April 1982.

[3] Brincker, R. *Note on the Random Decrement Technique.* Aalborg University, 1995.

[4] Brincker, R., Krenk, S., Kirkegaard, P.H. & Rytter A. *Identification of Dynamical Properties from Correlation Function Estimates.* Bygningsstatiske meddelelser. Vol. 63. No. 1., pp. 1-38, 1992.

[5] Brincker, R., Jensen, J.L. & Krenk, S. *Spectral Estimation by the Random Dec Technique.* Proc. 9th Int. Conf. on Experimental Mechanics, Copenhagen, Denmark, August 20-24, pp. 2049 -2058, 1990.

[6] Pandit, S.M. *Modal and Spectrum Analysis: Data Dependent Systems in State Space.* John Wiley & Sons, Inc. 1991.

[7] MATLAB User Guide, MATH WORKS Inc.

FRACTURE AND DYNAMICS PAPERS

PAPER NO. 37: A. Rytter, R. Brincker & P. H. Kirkegaard: *An Experimental Study of the Modal Parameters of a Damaged Cantilever.* ISSN 0902-7513 R9230.

PAPER NO. 38: P. H. Kirkegaard: *Cost Optimal System Identification Experiment Design.* ISSN 0902-7513 R9237.

PAPER NO. 39: P. H. Kirkegaard: *Optimal Selection of the Sampling Interval for Estimation of Modal Parameters by an ARMA-Model.* ISSN 0902-7513 R9238.

PAPER NO. 40: P. H. Kirkegaard & R. Brincker: *On the Optimal Location of Sensors for Parametric Identification of Linear Structural Systems.* ISSN 0902-7513 R9239.

PAPER NO. 41: P. H. Kirkegaard & A. Rytter: *Use of a Neural Network for Damage Detection and Location in a Steel Member.* ISSN 0902-7513 R9245

PAPER NO. 42: L. Gansted: *Analysis and Description of High-Cycle Stochastic Fatigue in Steel.* Ph.D.-Thesis. ISSN 0902-7513 R9135.

PAPER NO. 43: M. Krawczuk: *A New Finite Element for Static and Dynamic Analysis of Cracked Composite Beams.* ISSN 0902-7513 R9305.

PAPER NO. 44: A. Rytter: *Vibrational Based Inspection of Civil Engineering Structures.* Ph.D.-Thesis. ISSN 0902-7513 R9314.

PAPER NO. 45: P. H. Kirkegaard & A. Rytter: *An Experimental Study of the Modal Parameters of a Damaged Steel Mast.* ISSN 0902-7513 R9320.

PAPER NO. 46: P. H. Kirkegaard & A. Rytter: *An Experimental Study of a Steel Lattice Mast under Natural Excitation.* ISSN 0902-7513 R9326.

PAPER NO. 47: P. H. Kirkegaard & A. Rytter: *Use of Neural Networks for Damage Assessment in a Steel Mast.* ISSN 0902-7513 R9340.

PAPER NO. 48: R. Brincker, M. Demosthenous & G. C. Manos: *Estimation of the Coefficient of Restitution of Rocking Systems by the Random Decrement Technique.* ISSN 0902-7513 R9341.

PAPER NO. 49: L. Gansted: *Fatigue of Steel: Constant-Amplitude Load on CCT-Specimens.* ISSN 0902-7513 R9344.

PAPER NO. 50: P. H. Kirkegaard & A. Rytter: *Vibration Based Damage Assessment of a Cantilever using a Neural Network.* ISSN 0902-7513 R9345.

PAPER NO. 51: J. P. Ulfkjær, O. Hededal, I. B. Kroon & R. Brincker: *Simple Application of Fictitious Crack Model in Reinforced Concrete Beams.* ISSN 0902-7513 R9349.

PAPER NO. 52: J. P. Ulfkjær, O. Hededal, I. B. Kroon & R. Brincker: *Simple Application of Fictitious Crack Model in Reinforced Concrete Beams. Analysis and Experiments.* ISSN 0902-7513 R9350.

PAPER NO. 53: P. H. Kirkegaard & A. Rytter: *Vibration Based Damage Assessment of Civil Engineering Structures using Neural Networks.* ISSN 0902-7513 R9408.

FRACTURE AND DYNAMICS PAPERS

PAPER NO. 54: L. Gansted, R. Brincker & L. Pilegaard Hansen: *The Fracture Mechanical Markov Chain Fatigue Model Compared with Empirical Data.* ISSN 0902-7513 R9431.

PAPER NO. 55: P. H. Kirkegaard, S. R. K. Nielsen & H. I. Hansen: *Identification of Non-Linear Structures using Recurrent Neural Networks.* ISSN 0902-7513 R9432.

PAPER NO. 56: R. Brincker, P. H. Kirkegaard, P. Andersen & M. E. Martinez: *Damage Detection in an Offshore Structure.* ISSN 0902-7513 R9434.

PAPER NO. 57: P. H. Kirkegaard, S. R. K. Nielsen & H. I. Hansen: *Structural Identification by Extended Kalman Filtering and a Recurrent Neural Network.* ISSN 0902-7513 R9433.

PAPER NO. 58: P. Andersen, R. Brincker, P. H. Kirkegaard: *On the Uncertainty of Identification of Civil Engineering Structures using ARMA Models.* ISSN 0902-7513 R9437.

PAPER NO. 59: P. H. Kirkegaard & A. Rytter: *A Comparative Study of Three Vibration Based Damage Assessment Techniques.* ISSN 0902-7513 R9435.

PAPER NO. 60: P. H. Kirkegaard, J. C. Asmussen, P. Andersen & R. Brincker: *An Experimental Study of an Offshore Platform.* ISSN 0902-7513 R9441.

PAPER NO. 61: R. Brincker, P. Andersen, P. H. Kirkegaard, J. P. Ulfkjær: *Damage Detection in Laboratory Concrete Beams.* ISSN 0902-7513 R9458.

PAPER NO. 62: R. Brincker, J. Simonsen, W. Hansen: *Some Aspects of Formation of Cracks in FRC with Main Reinforcement.* ISSN 0902-7513 R9506.

PAPER NO. 63: R. Brincker, J. P. Ulfkjær, P. Adamsen, L. Langvad, R. Toft: *Analytical Model for Hook Anchor Pull-out.* ISSN 0902-7513 R9511.

PAPER NO. 64: P. S. Skjærbæk, S. R. K. Nielsen, A. Ş. Çakmak: *Assessment of Damage in Seismically Excited RC-Structures from a Single Measured Response.* ISSN 1395-7953 R9528.

PAPER NO. 65: J. C. Asmussen, S. R. Ibrahim, R. Brincker: *Random Decrement and Regression Analysis of Traffic Responses of Bridges.* ISSN 1395-7953 R9529.

PAPER NO. 66: R. Brincker, P. Andersen, M. E. Martinez, F. Tallavó: *Modal Analysis of an Offshore Platform using Two Different ARMA Approaches.* ISSN 1395-7953 R9531.

PAPER NO. 67: J. C. Asmussen, R. Brincker: *Estimation of Frequency Response Functions by Random Decrement.* ISSN 1395-7953 R9532.

Department of Building Technology and Structural Engineering
Aalborg University, Sohngaardsholmsvej 57, DK 9000 Aalborg
Telephone: +45 98 15 85 22 Telefax: +45 98 14 82 43